Shockwave–boundary layer interaction control by plasma aerodynamic actuation: An experimental investigation*

Sun Quan(孙 权)†, Cui Wei(崔 巍), Li Ying-Hong(李应红), Cheng Bang-Qin(程邦勤), Jin Di(金 迪), and Li Jun(李 军)

Science and Technology on Plasma Dynamics Laboratory, Air Force Engineering University, Xi'an 710038, *China*

(Received 17 December 2013; revised manuscript received 7 March 2014; published online 22 May 2014)

The potential of controlling shockwave–boundary layer interactions (SWBLIs) in air by plasma aerodynamic actuation is demonstrated. Experiments are conducted in a Mach 3 in-draft air tunnel. The separation-inducing shock is generated with a diamond-shaped shockwave generator located on the wall opposite to the surface electrodes, and the flow properties are studied with schlieren imaging and static wall pressure probes. The measurements show that the separation phenomenon is weakened with the plasma aerodynamic actuation, which is observed to have significant control authority over the interaction. The main effect is the displacement of the reflected shock. Perturbations of incident and reflected oblique shocks interacting with the separation bubble in a rectangular cross section supersonic test section are produced by the plasma actuation. This interaction results in a reduction of the separation bubble size, as detected by phase-lock schlieren images. The measured static wall pressure also shows that the separation-inducing shock is restrained. Our results suggest that the boundary layer separation control through heating is the primary control mechanism.

Keywords: shock, boundary layer, plasma, flow control

PACS: 52.50.Nr, 52.80.Mg, 47.80.Jk **DOI:** 10.1088/1674-1056/23/7/075210

1. Introduction

Shockwave–boundary layer interactions (SWBLIs) commonly occur in high-speed flows from the transonic to hypersonic regime.[1,2] They can be found in a variety of applications including transonic wings, axial turbines, and mixed-compression inlets. The interaction between the shock and the boundary layer on the inlet walls can cause the boundary layer to separate. The resultant separated flow alters the local flow characteristics and induces the shock to move forward. Whenever this sequence of events becomes self-reinforcing, the normal shock can move out of the inlet and cause an inlet un-start.

The boundary layer separation control can be achieved by using many different approaches, all of which modify the flow near the surface. The flow control is typically provided by mechanisms which energize the boundary layer by introducing a higher speed flow near the wall. Such devices involve blowing, bleeding, or mixing of the inlet flow. Blowing and bleed based approaches have been shown to work well, but at the cost of introducing losses that result from the additional, and frequently significant, weight of the required ducting systems, duct drag, and engine losses. The most successful method of passive separation suppression is through the use of low profile vortex generators (VGs). Although VGs are generally successful in delaying the flow separation, they also incur considerable additional drag and reduce the inlet total pressure recovery.

Compared with blowing/suction, vortex generators, and other conventional flow control methods, the plasma flow control have the remarkable advantages of simple structure, flexible control, and large excitation frequency bandwidth. It has become a hot topic in the international aerodynamics and thermodynamics field.[3–9] Recently, localized arc filament plasma actuators (LAFPAs) were developed at the Ohio State University as a means to introduce strong, tailored, high frequency perturbations to the flow.[10–12] They forced the incoming boundary layer at a frequency close to one of the instability frequencies associated with the reflected shock interacting with the unsteady separation bubble. This resulted in a reduction of both the separation bubble size and the reflected shock unsteadiness. Another approach used a pulsed plasma jet to force an oblique shock on a compression ramp in a Mach 3 flow.[13] It was reported that the convection of thermal spots in the incoming boundary layer displaces the oblique shock location upstream, while forcing in the separation bubble did not produce a detectable effect. Separation bubble forcing was also performed using a magnetically driven gliding arc to modify the static pressure distributions downstream and modulate the flow in the separation region.[14] Flow forcing by repetitive thermal perturbations in NS-DBD actuators was consistent with the high-speed flow control mechanism used in repetitively localized arc filament plasma actuators.[15] The main idea of this approach is forcing the flow with high-amplitude, high-bandwidth perturbations, at a frequency approaching one

*Project supported by the Key Program of the National Natural Science Foundation of China (Grant No. 51336011) and the National Natural Science Foundation of China (Grant Nos. 51207169 and 51276197).

†Corresponding author. E-mail: steve5761@126.com

© 2014 Chinese Physical Society and IOP Publishing Ltd

of the flow instability frequencies, thus triggering the subsequent growth in the flow. These results suggest that plasma-induced SWBLI flow forcing may have potential for high-speed flow control applications.

Arc plasma actuators have also been developed at the Science and Technology on Plasma Dynamics Laboratory at the Air Force Engineering University in China. Originally, these actuators were developed to control the shock in a supersonic flow. Experimental results showed that the plasma aerodynamic actuation can reduce the intensity of the shock in a supersonic flow.[16–18] In the present work, a detailed investigation of the effect of actuator placement and frequency on the control authority indicates that the actuators' primary control mechanism is heating by plasma discharge, as evidenced by schlieren imaging and static wall pressure probes.

2. Experimental setups

The design Mach number of the small-scale short-duration supersonic wind tunnel is 3 and its steady operation time is about 60 ms. The test section is rectangular, 80 mm wide and 50 mm high. The gas static pressure and total temperature in the test section are 3000 Pa and 300 K, respectively. A groove in the test section lower wall is designed for the plasma actuator fabrication. The shock generator used in the present experiments is a 15° and 10 mm long ramp.

A pulsed-DC power supply is adopted, the output voltage ranges from 0 kV to 20 kV, and the repetition frequency varies from 100 Hz to 2000 Hz. The plasma actuator consists of copper electrodes and a boron-nitride (BN) ceramic dielectric material. The six cylindrical copper electrodes embedded in the BN ceramic are arranged as three pairs with cathode–anode intervals of 5 mm. The upper flow surfaces of the electrodes and the ceramic are plated to ensure no unintentional shock wave generation in the test section lower wall.

The test system consists of a gas pressure measurement system, a schlieren system, and an arc discharge voltage–current measurement system. Along the supersonic flow direction, there are three pressure dots which cover the interaction area of the shock wave and the boundary layer. The schlieren system uses a high-speed CCD camera with a maximum frame rate of 200000 fps. For the purpose of acquiring the pulsed discharge process, the frame rate in this paper is selected as 20000 fps (frame interval of 50 μs), and the resolution is 512×218 pixels. The camera is triggered by a Stanford Research System DG535 delay/pulse generator. When the discharge initiates and is detected by the TCP312 current probe, a signal will be generated and transmitted from the oscilloscope to the DG535 generator, after receiving it, the DG535 generator outputs a level signal to start the camera with a preset delay. The schematic diagram of the plasma actuator and the experimental setup are shown in Figs. 1 and 2, respectively.

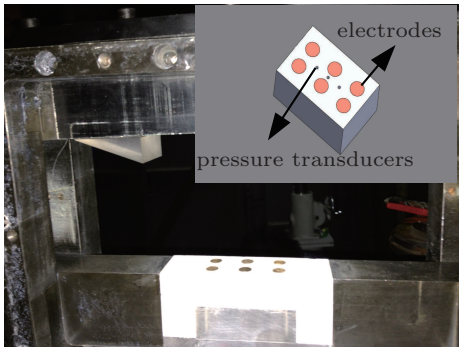


Fig. 1. (color online) Test section schematic diagram with compression ramp model installed.

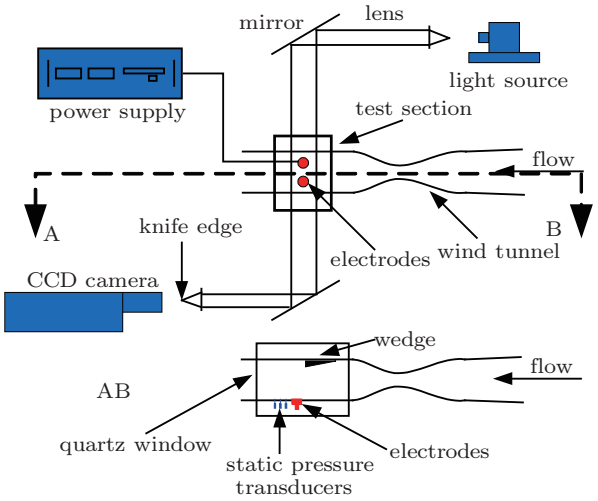


Fig. 2. (color online) Schematic diagram of experimental setup.

3. Experimental results

3.1. Electrical characteristics

From Fig. 3, we can see that the discharge arc is strongly bounded near the wall surface. The inner layer of the discharge arc is white, which indicates that the plasma temperature is very high. The outer layer is blue and purple because of its weak discharge intensity.

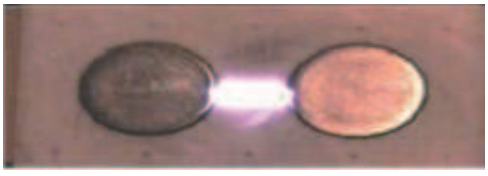


Fig. 3. (color online) Image of arc discharge from top view.

The pulse frequency and the discharge voltage are 1 kHz and 15 kV, respectively. The single-period discharge voltage–current curves are shown in Fig. 4. The discharge process in Fig. 5 contains a breakdown process and a DC hold-up

process. The power supply is designed to output a negative pulse. When the gas breakdown takes place, the voltage reduces sharply from about 15 kV to 0.5 kV within 200 ns. The discharge current abruptly reaches as high as 40 A within 600 ns, and gradually falls back; the duration of a single pulse lasts about 6 μs. As the voltage maintains about 500 V, the power is still no more than 50 kW.

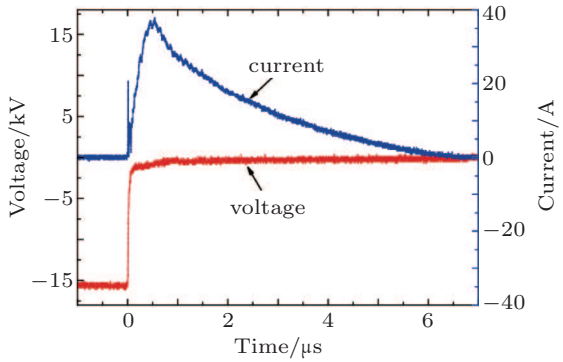


Fig. 4. (color online) The V–I plot with discharge frequency of 1 kHz and voltage of 15 kV.

3.2. Flow field characteristics

3.2.1. Different actuation positions

The actuators can be placed in three locations relative to the SWBLIs in Fig. 5: just upstream of the front leg of the lambda shock (case 1), within the interaction bubble (case 2), and just downstream of the front leg of the lambda shock (case 3).

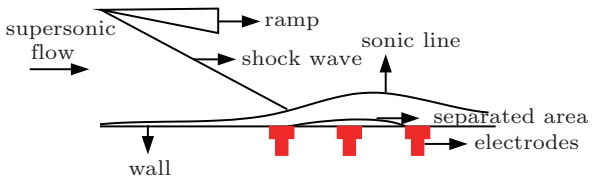


Fig. 5. (color online) Different placements of plasma actuators.

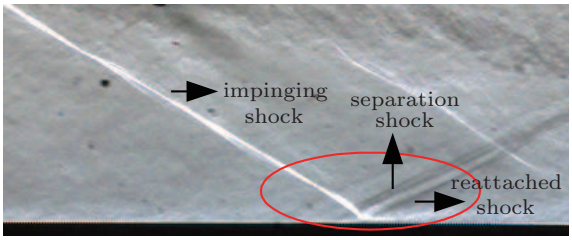


Fig. 6. (color online) The baseline flow field with impinging shock.

Figure 6 shows one phase-locked schlieren image of the baseline flow. The flow Mach is 3, the ramp is 15°, which is consistent with the oblique shock angle of 32°. In the image, the incident shock, the reflected shock, and the flow separation region near the bottom wall can be identified clearly. The impinging shock front disappears at the intersection with the sonic line, encompassing the separated flow region. The incoming boundary layer on the lower wall appears to be turbulent, with a boundary layer thickness of approximately 3 mm. Figures 7(b)–7(d) show three phase-locked schlieren images taken when the flow is forced by the plasma actuator at the pulse repetition rate of 1 kHz.

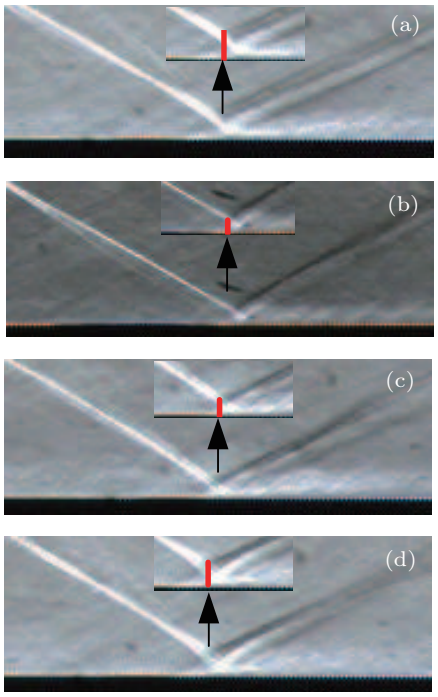


Fig. 7. (color online) The schlieren images with and without plasma actuation: (a) the baseline flow, (b) with upstream plasma actuation, (c) with separation bubble plasma actuation, (d) with downstream plasma actuation.

In the case of an oblique shockwave generated using a 15° ramp, there exist strong separation and upstream plasma actuation (case 1), resulting in increased recirculation as expected. The separation bubble plasma actuation (case 2) shows some important changes in the structure of the recirculation zone. While the downstream plasma actuation (case 3) does not show a significant change in the schlieren image. Figure 7 shows four schlieren images taken with and without plasma actuation. The length l, marked by the arrows in the tops of the images, is the distance between the incoming oblique shock interacting with the first of the compression waves to the bottom wall. It can be seen that in the presence of upstream plasma actuation and separation bubble plasma actuation, the length is shorter than that in the absence of plasma actuation or in the presence of downstream plasma actuation. These results show that the arc plasma can restrain or delay the separation when applying the plasma actuation upstream or at the separation bubble.

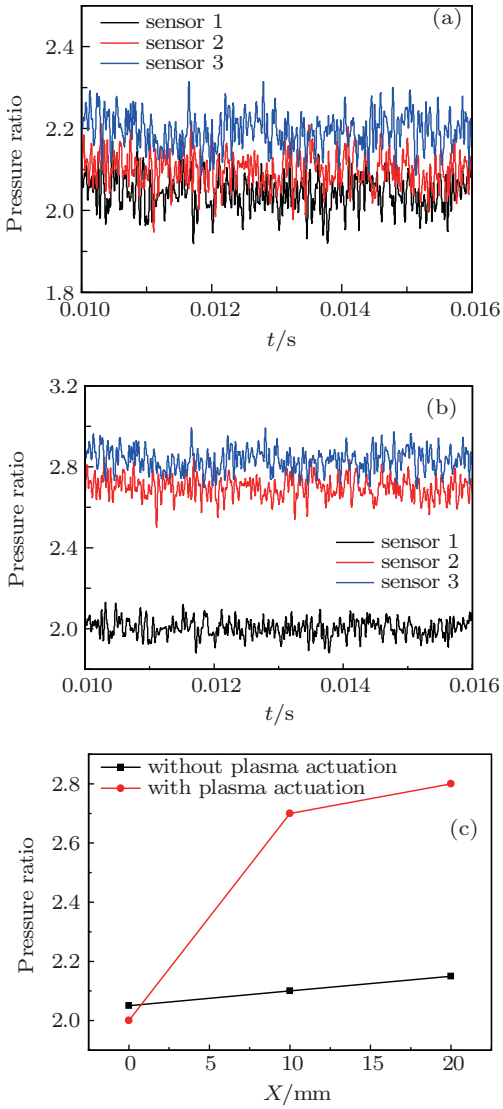


Fig. 8. (color online) Pressures in the wall separation area: (a) baseline, (b) with plasma actuation, (c) comparison of wall pressures.

An oblique shock generated from a 15° ramp interacting with the boundary layer, on the other hand, does induce a recirculation bubble and separation. This is verified by the schlieren image of the interaction zone, which shows that the reflected shock appears significantly upstream of the point where the incoming oblique shock hits the boundary layer. The static pressure is measured using wall pressure taps. The response frequency of the pressure transducers is 100 kHz. Along the supersonic flow direction, there are three pressure dots (sensor 1, sensor 2, and sensor 3) which cover the interaction area of the shock wave and the boundary layer. The flow is forced by the upstream arc plasma actuation at the pulse repetition rate of 1 kHz. In Fig. 8(a), the pressures on the three sensors are approximately the same. This result indicates that the flow is separated due to the interaction with the impinging shock. When applying the plasma aerodynamic actuation, the pressure increases along the supersonic flow as shown in Fig. 8(b). In Fig. 8(c), the baseline wall static pressure profile is compared with the plasma actuation. The baseline pressure is a plateau, which indicates that the flow is separated due to the interaction. The slope increases rapidly as the actuation is applied compared with the baseline. The effect of the plasma actuation becomes more apparent and results in a significant modification of the static wall pressure profile. It also indicates that the pressure record does not figure pressure oscillations corresponding to the power release. The reason is as follows. From the V–I characteristic (Fig. 4), we know that the time duration of the plasma discharge is only 6 μs, while the response frequency of the pressure transducer is 100 kHz. So we can hardly observe the variation of the wall static pressure in the discharge process. The static pressure measured is the macroscopic patterns of the flow field.

3.2.2. Different actuation frequencies

Natural unsteadiness has long been observed and studied in SWBLIs, especially when the separation occurs. Low frequency and large amplitude unsteadiness of a broadband nature has been observed in the region around the foot of the reflected shock. The actuators are found to have the best control authority when they are located upstream of the front leg of the primary-reflected shock structure, or the lambda shock structure. This location allows the actuators to energize the boundary layer before it encounters the front leg of the lambda shock. The actuators are operated at several different forcing frequencies (800 Hz, 1000 Hz, 1200 Hz, 1500 Hz, and 2000 Hz) at this location to determine the parameter space location of the best control authority. Figure 9 shows six phase-locked schlieren images of the unsteady flow structure.

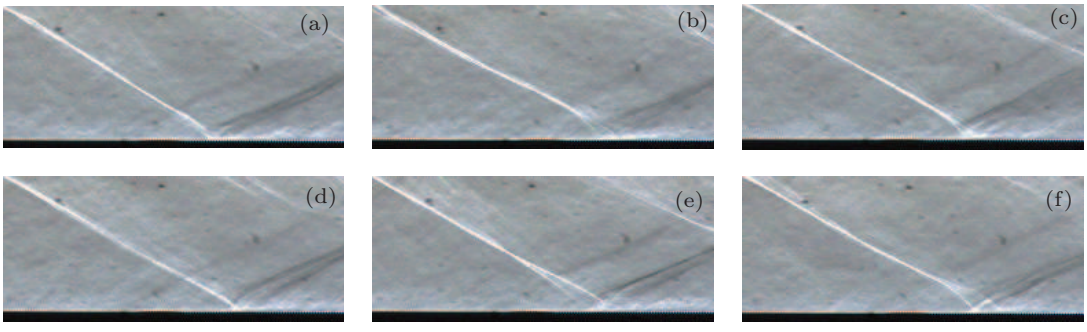


Fig. 9. Unsteady flow structure without actuation: (a) $T = 0$ μs, (b) $T = 100$ μs, (c) $T = 200$ μs, (d) $T = 400$ μs, (e) $T = 500$ μs, (f) $T = 1000$ μs.

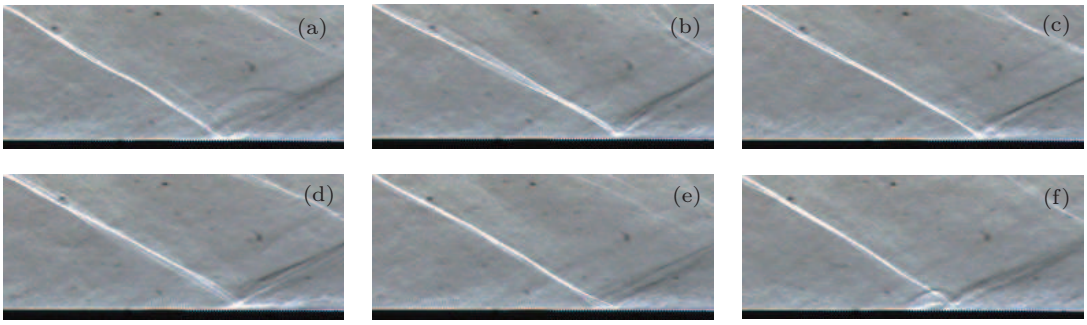


Fig. 10. (color online) Unsteady flow structure with 1 kHz plasma actuation: (a) $T = 0$ μs, (b) $T = 100$ μs, (c) $T = 200$ μs, (d) $T = 400$ μs, (e) $T = 500$ μs, (f) $T = 1000$ μs.

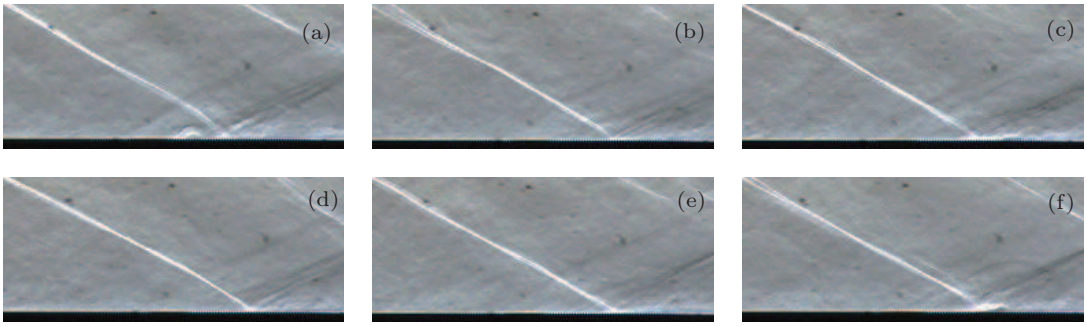


Fig. 11. (color online) Unsteady flow structure with 2 kHz plasma actuation: (a) $T = 0$ μs, (b) $T = 100$ μs, (c) $T = 200$ μs, (d) $T = 400$ μs, (e) $T = 500$ μs, (f) $T = 1000$ μs.

The impinging shock induces a recirculation bubble and separation. The flow is forced by the upstream arc plasma actuation at the pulse repetition rate of 1 kHz or 2 kHz. The images in Figs. 10 and 11 are taken at 10 μs after the discharge pulse. From the flow structure picture, we can see that the separation phenomenon is weakened when applying the upstream plasma actuation. There appears to be no resonance or optimal frequency associated with this actuator. Due to the limit of the plasma power frequency (only 0.1–2 kHz), we conjecture that this would require a higher forcing frequency. Further studies at higher frequencies are necessary.

4. Numerical simulations

We perform a numerical simulation using a structured grid based on the discretization of the unsteady compressible Navier–Stokes (N–S) equations with an explicit cell-centered finite volume method. The turbulence model uses the Reynolds stress five-equation model and the enhanced wall treatment method. Our numerical validation for SWBLIs is compared with the published results.[19] A 10°, 300 mm long shock generator plate is used to generate an oblique shock impinging on an opposite 500 mm long flat plate. The supersonic flow is 5 Mach. The static temperature is 738 K and the static pressure is 6.896 kPa. Figures 12 and 13 show that the current simulation results agree with the published simulation and experimental results.[19]

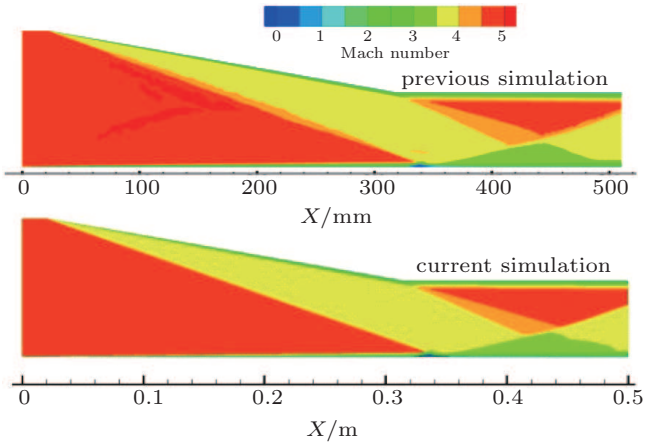


Fig. 12. (color online) Current simulation results compared with the published simulation results.

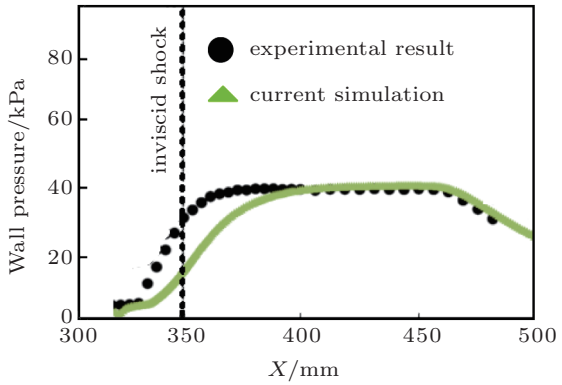


Fig. 13. (color online) Current simulation results compared with the experimental results.

Based on the results of our experiment, the flow Mach is 3 and the ramp is 15°. In order to acquire a thick boundary layer, a 15° shock generator plate is used to generate an oblique shock impinging on an opposite 4700 mm long flat plate. The incident shock impinging point is marked as $X = 0$ for the inviscid state. The discharge voltage–current curves are shown in Fig. 4. The arc discharge lasts about 6 μs. In this process, the voltage maintains 500 V and the current peaks at 40 A. The average discharge power is 10 kW. In this paper, the source term of the arc plasma is set in the form of the average power density added in the N–S equations. The simplified rectangular thermal area is 20 mm wide and 5 mm high from the arc discharge picture. So the average power is about 10^{11} W/m^3. The plasma actuator is placed upstream of the separation area.

Figure 14 shows the static pressure distribution contour without and with the plasma aerodynamic actuation (the upper picture is the benchmark flow). From the picture, we can clearly observe the incident shock, the expansion fan, the reflected shock, and the flow separation region near the bottom wall without the plasma actuation. When applying the plasma actuation, the flow separation region is weakened and the strength of the reflected shock is reduced. This result indicates that the flow separation of SWBLIs is controlled by the energy added through the plasma aerodynamic actuation.

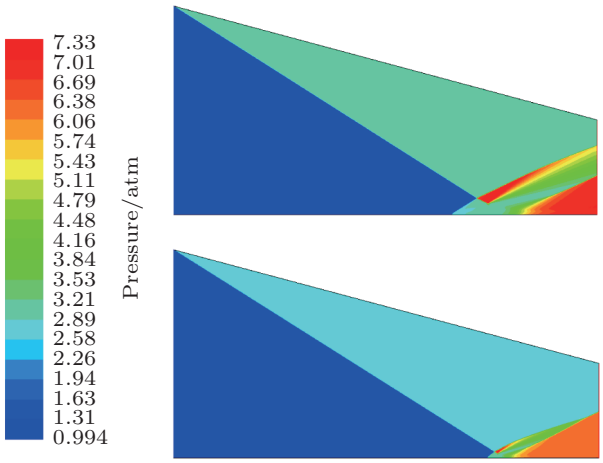


Fig. 14. (color online) Static pressure contour for SWBLIs.

Figure 15 shows the Mach number and the static pressure distributions on the surface ($Y = 0.2$ m). From the benchmark flow, we can observe three increases in pressure (three Mach number reductions) and one pressure reduction (one Mach number increase). These phenomena show that the flow passes through the incident shock, the separated shock, the expand fan, and the attached shock. They also show that a strong flow separation occurs. When applying the plasma actuation, we can observe three pressure increases (three Mach number reductions); both the increment and the duration of the pressure reduction (Mach number increase) are very small. This indicates that the flow separation is controlled.

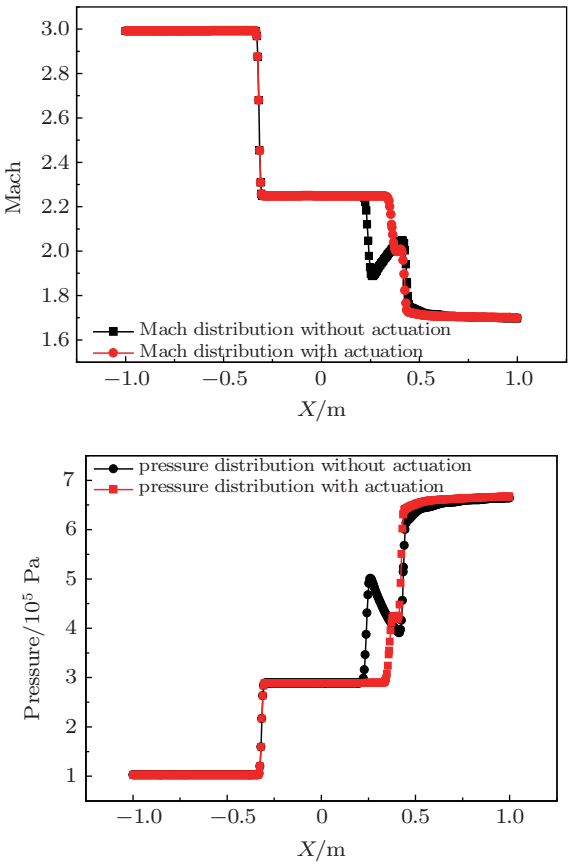


Fig. 15. (color online) (a) The Mach number and (b) the static pressure distributions on the surface ($Y = 0.2$ m).

5. Discussion

The plasma aerodynamic actuator phenomenon has drawn increasing attention worldwide for its potential application in both low and high speed flow controls. There are three widely accepted mechanisms of plasma flow control, which could be listed as follows: (i) electrohydrodynamics (EHD) forcing driven by the momentum transfer between neutral background gas molecules and charged particles drifting in an electric field, (ii) magnetohydrodynamics (MHD) forcing achieved when an external magnetic field is applied to charged particles and creates a Lorentz force, (iii) localized gas heating that creates fast and strong disturbance or virtual shape to change the flow structure. It is generally believed that in a low speed flow, the electrostatic force plays an important role, while in a supersonic flow, the heating mechanism may be more convincing.

5.1. Heating effect of plasma discharge

The dominating mechanism may be varied for different plasma sources or actuators. In this paper, the discharge voltage–current curves are shown in Fig. 4. The source term of the arc plasma is set in the form of the average power den-

sity. When applying the arc plasma actuation, there is a special plasma layer inside the boundary layer with its temperature as high as 3000 K as shown in Fig. 16(a). The high temperature plasma generation changes the pressure and the temperature in the near-wall region, forming a virtual aerodynamic surface in the supersonic air stream. The arc plasma produced by the high voltage DC discharge can induce a shock in the supersonic flow and deflect the air flow after the shock (see Fig. 16(b)). It can also change the position and the angle of the original shock. This mechanism is considered to be a Joule heating action of the DC discharge, that is, a heating choke effect.

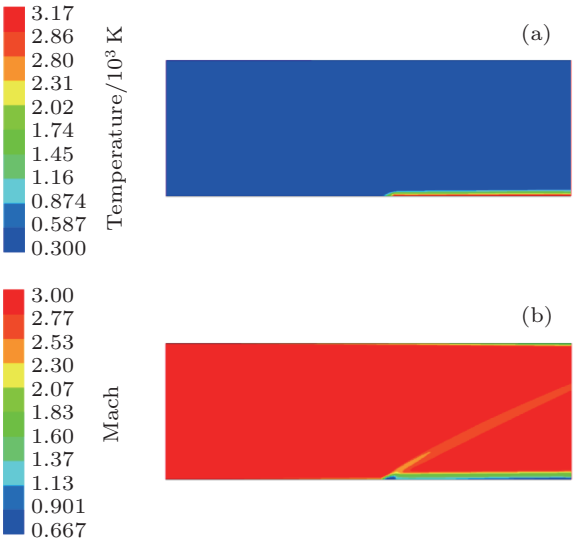


Fig. 16. (color online) Shock wave induced by energy added in supersonic flow: (a) static temperature distribution contour, (b) Mach number distribution contour.

The present study indicates that the plasma actuator method is effective in controlling SWBLIs by means of a precompression effect at the windward side of the virtual aerodynamic surface, a weakening effect on the reflected shock, and an accelerating effect on the boundary layer flow of the expansion wave. When the shock impingement position is near the expansion wave generating area at the leeward side of the virtual aerodynamic surface, the size of the separation bubble is greatly reduced.

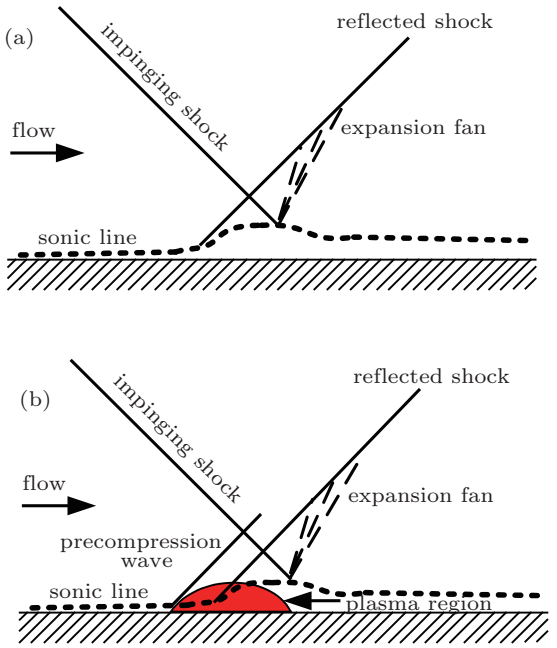


Fig. 17. (color online) Sketch map of SWBLI control by plasma actuator: (a) sketch map of SWBLIs, (b) sketch map of SWBLIs with actuation.

5.2. Impact effect of plasma discharge

During the experiment, another interesting phenomenon drew our attention. The previous work confirmed compression waves generated by the arc plasma in a quiescent atmosphere. Figure 18 shows six phase-locked schlieren images taken when the flow is forced by the upstream arc plasma actuation at the pulse repetition rate of 1 kHz. Because the discharging pulse durations are 6 μs and the interval of two phase-locked schlieren images is 50 μs, the compression wave can be observed only once in every period. The compression wave generated by the pulse discharge in the actuator is readily apparent in the supersonic flow. The propagating compression wave produced by the discharge disturbs the oblique shock wave, and results in a perturbation when traveling along the shock. As we all know, low-frequency and large-amplitude unsteadiness of a broadband nature has been observed in the

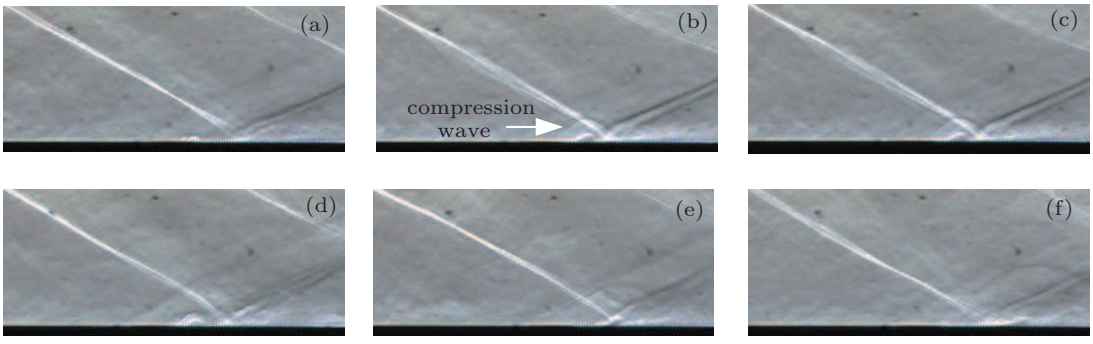


Fig. 18. Compression wave induced in a supersonic flow: (a) $T = 0$ μs, (b) $T = 1000$ μs, (c) $T = 2000$ μs, (d) $T = 3000$ μs, (e) $T = 4000$ μs, (f) $T = 5000$ μs.

region around the foot of the reflected shock. When the actuation frequency of the plasma shock is consistent with the natural oscillation frequency of SWBLIs, the plasma shock may control the separation of the boundary layer. Due to the present limit of the plasma power frequency (only 0.1–2 kHz), further studies at higher frequencies are required to validate this idea.

6. Conclusion

Experimental investigations on controlling the separation of the boundary layer by an impinging shock were performed in a small-scale short-duration supersonic wind tunnel. The actuators were placed in three locations relative to the SWBLIs: just upstream of the front leg of the lambda shock, within the interaction bubble, and just downstream of the front leg of the lambda shock. Through the results of schlieren imaging and static wall pressure probes, some conclusions can be acquired as follows. (i) The separation phenomenon is weakened when applying the plasma actuation upstream. (ii) The static wall pressure measurements also show that the separation-inducing shock is restrained. (iii) The compression wave is observed to be induced by an arc discharge not only in a quiescent atmosphere but also in a supersonic flow. (iv) The boundary layer separation control through heating is the primary control mechanism.

References

[1] Dussauge J P, Dupont P and Debieve J F 2006 *Aerospace Sci. Tech.* **10** 85

[2] Andrew P L and Werner J A 2011 *Exp. Fluids* **50** 89

[3] Roth J R 2003 *Phys. Plasmas* **5** 2117

[4] Enloe C L, McLaughlin T E and VanDyken R D 2004 *AIAA J.* **42** 589

[5] Porter C O, Baughn J W and McLaughlin 2007 *AIAA J.* **45** 1562

[6] Post M L and Corke T C 2006 *AIAA J.* **44** 3125

[7] Ni G H, Meng Y D, Cheng C and Lan Y 2010 *Chin. Phys. Lett.* **27** 055203

[8] Pan W X, Li T, Meng X, Chen X and Wu C K 2005 *Chin. Phys. Lett.* **22** 2895

[9] Li L C and Xia W D 2008 *Chin. Phys. B* **17** 649

[10] Webb N, Clifford C and Samimy M 2013 51rd *AIAA Aerospace Sciences Meeting including the New Horizons Forum and Aerospace Exposition,* January 7–10, 2013 Texas, USA

[11] Webb N, Clifford C and Samimy M 2012 6rd *AIAA Flow Control Conference,* June 25–28, 2012 New Orleans, USA

[12] Webb N, Clifford C and Samimy M 2011 41rd *AIAA Fluid Dynamics Conference and Exhibit,* June 27–30, 2011 Hawaii, USA

[13] Narayanaswamy V, Raja L L and Clemens 2012 *Phys. Fluids* **24** 076101

[14] Kalra C S, Zaidi S, Scheider M N and Miles R B 2009 47rd *AIAA Aerospace Sciences Meeting Including the New Horizons Forum and Aerospace Exposition,* January 5–8, 2009 Florida, USA

[15] Nishihara M D and Adamovich I V 2013 51rd *AIAA Aerospace Sciences Meeting including the New Horizons Forum and Aerospace Exposition,* January 7–10, 2013 Texas, USA

[16] Sun Q, Cheng B Q and Li Y H 2013 *Plasma Sci. Technol.* **15** 908

[17] Sun Q, Cheng B Q and Li Y H 2013 *Sci. China-Technol. Sci.* **56** 795

[18] Wang J, Li Y H and Xing F 2009 *J. Appl. Phys.* **106** 03307

[19] Shang J S, Hankey W L and Law C H 1976 *AIAA J.* **14** 1451